Title: Real-space Orbital-selective Probing of the Cooper Pairing in Iron Pnictides

Authors: J.-X. Yin[1,2], Ang Li[2,6], X. -X. Wu[1], Jian Li[2], Zheng Wu[2], J.-H. Wang[2], C.-S. Ting[2], P.-H. Hor[2], X. J. Liang[1], C. L. Zhang[3], P. C. Dai[3], X. C. Wang[1], C. Q. Jin[1,7], G. F. Chen[1], J. P. Hu[1,4], Z. -Q. Wang[5], H. Ding[1,7], S. H. Pan[1,2,7]†

Affiliations:

[1]Institute of Physics, Chinese Academy of Sciences, Beijing 100190, China.

[2]TCSUH and Department of Physics, University of Houston, Houston, Texas 77204, USA.

[3]Department of Physics and Astronomy, Rice University, Houston, Texas 77005, USA.

[4]Department of Physics, Purdue University, West Lafayette, Indiana 47907, USA.

[5]Department of Physics, Boston College, Chestnut Hill, Massachusetts 02467, USA.

[6]Shanghai Institute of Microsystem and Information Technology, Chinese Academy of Sciences, Shanghai 200050, China.

[7]Collaborative Innovation Center of Quantum Matter, Beijing, China

†Corresponding author. E-mail: span@iphy.ac.cn.

One of the basic features of iron-based superconductors is the multi-orbital nature[1-5]. In momentum space, the multi-orbital nature of the iron-based superconductivity manifests itself as the Fermi sheet dependence of the Cooper pairing strength. Here we report a real-space study, using scanning tunnelling microscopy/spectroscopy (STM/S), on the Cooper pairing in $Ba_{0.6}K_{0.4}Fe_2As_2$ and

LiFeAs single crystals. On different terminating surfaces with their distinct atomic identities[6], we have observed different types of fully opened superconducting gap structures. Symmetry analysis on the Fe3d-As4p orbital hybridization suggests that the tunnelling on different terminating surfaces probes different Fe3d orbitals. Therefore, the phenomenon of the surface dependent gap structures essentially demonstrates the orbital feature of the Cooper pairing in the Fe-As layer.

As the copper-oxide plane to the cuprates superconductivity, the iron-arsenic trilayer is generally considered to be the key structure responsible for the emergence of superconductivity in the iron pnictides. Different from the copper-oxide plane in cuprates which has a single Fermi sheet involving the Cu $d_{x^2-y^2}$ orbital[7], the iron-asenic trilayer in pnictides has multiple FS sheets involving all the t_{2g} Fe d-orbitals[1-3]. Therefore, the orbital dependence of the electron pairing is one of the essential issues in understanding the iron-based superconductivity. The K-doped $BaFe_2As_2$ and LiFeAs are ideal materials to investigate this problem due to their stoichiometric Fe-As layers and high superconductivity volume fraction. However, the active surface K atoms could lead to lattice disorder for K-doped Ba122 materials[8-10], while native impurities could be easily introduced during growth of LiFeAs materials[11-13]. Both the surface disorder and native impurities can potentially affect the Fe-As integrity and modify its superconducting properties[14]. Using cryogenic *in situ* cleaving technique, we have obtained ordered surfaces with clear atomic identities in $Ba_{0.6}K_{0.4}Fe_2As_2$[6]. With the persistent effort to enhance the sample quality, LiFeAs single crystals free from defects

for a large field of view are currently available. A high-resolution measurement of the superconducting gap on these ordered and clean surfaces is highly demanded, as it will help us to understand the intrinsic features of the electron pairing.

As illustrated in Fig. 1a and b, Cleavage of $Ba_{0.6}K_{0.4}Fe_2As_2$ single crystals mainly breaks the As-Ba(K) bonding, generating the Ba(K)-terminating surface with $\sqrt{2}\times\sqrt{2}R45°$ reconstruction (rt2) or the As-terminating surface with 1×2 reconstruction (dimmer rows)(ref. 6). Besides of these two ordered surfaces, we also observe a disordered surface, which is supposed to be caused by the active K atoms. Such surface exhibits an inhomogeneous superconducting gap varying from 2 meV to 10 meV in the gap-map and line-cut spectrums (Figs. 1c-e), coinciding with the spectra reported by previous STM study without atomic resolution[8-10]. However, such a large inhomogeneity of the gap sizes is inconsistent with results on other iron-based superconductors with ordered terminating surfaces[14], and the values of the energy gaps are smaller than those from ARPES measurements on the same material[15,4]. These discrepancies suggest that parts of the spectral features shown on the disordered surface are unlikely to be the intrinsic properties of the Fe-As layer and the disorder/impurity effects may play a role[13].

In contrast to the disordered surface, the gap magnitudes observed on the As-terminating and Ba(K)-terminating surfaces are quite homogeneous in each case, and we further find that their gap structures are surprisingly different between each other.

Along the line draw in Fig. 2a, we take spectrums from the Ba(K)-terminating region to the As-terminating region as shown in Fig. 2b. The superconducting gap is 6.0 meV deep inside the Ba(K)-terminating region and 10.5 meV inside the As-terminating region. Interestingly, the spectra along the boundary of the two regions have much broader coherent peaks, possibly due to the electronic decoherence caused by the step-edge scattering. From the gap-maps on the As and the Ba(K) regions (Figs. 2c and d), one can find that the gap only varies less than 1.0 meV on each surface, demonstrating the spatial homogeneity of the electron pairing strength.

Outside the superconducting coherent peaks, there are clear additional peaks observed in the spectra on all surfaces. Notably, their positions are always symmetrically located around ±18 meV, despite the different superconducting gap sizes. The shape of these additional peaks resembles the dip-hump structure in cuprates[16]. One possible reason for this behavior is the coupling effect with the (π, π) magnetic resonant mode[10,17]. Accordingly, the peak energy should roughly equals to the mode energy plus the gap energy. It is puzzling that this extra peak remains constant despite the large difference of the gap sizes, which would suggest the large difference in the mode energies for the two regions, possibly due to the anti-correlation effect between the mode energy and the gap energy[10]. It is also conceivable that the bosonic mode may couple to the global gap function[4] rather than any specific local gap channel in this multi-gap system.

To explore the fine structures of the energy gap on the ordered surfaces, we

measure the spectra at a much lower temperature as displayed in Fig. 2e. Clearly, both spectra are stateless near the zero-energy, which directly excludes any nodal symmetry of the electron pairing. Taking a closer look at the spectrum on the Ba(K)/As surface, we can find that there is an extra bump at 10.5/6 meV as marked by the arrows, which coincides with the energy of the coherent peak on As/Ba(K) surface. These bumps, together with the coherent peaks, form a similar two-gap structure but with different spectral weights on each surface.

The two-gap structure is also captured in LiFeAs material, while it behaves as a different type of form. Due to the weak bonding between two Li layers, LiFeAs has only one cleaving surface, as illustrated in Fig. 3a. In Fig. 3b we present an image of a large defect-free Li terminated surface. When we zoom into a small area, there is one lower As atom between four surface Li atoms, which is consistent with the subatomic distance between the As and Li layers in bulk (~ 0.5 Å). The line-cut spectra shown in Fig. 3c demonstrate a spatially uniform (extremely homogenous) and fully-opened gap in this system. Measuring at a much lower temperature, we observe a clear double-gap structure as shown in Fig. 3d. As compared with the spectra taken on the samples with more native impurities/defects, its spectral bottom is flatter and the coherent peaks of the small gap are more evident.

In order to directly associate these diverse gap structures with the iron-based superconductivity, we re-plot the spectra on each surface in the energy unit of $k_B T_C$ in

Fig. 4a. For both materials, the ratio $2\Delta/k_BT_C$ of the small gap is around 4 while for the large gap around 7. Both these numbers are larger than the BCS value 3.5, implying a strong coupling superconducting ground state. Besides the superconducting coherent peaks, there is also a narrower flat bottom characterizing each of their gap structures, with its energy range around $2k_BT_C$ for both materials. It matches the value derived from the transport measurements[18], since these probes are especially sensitive to the stateless region. Existence of such a smaller flat bottom than the gap coherent peak-peak distance may be due to the anisotropy of the superconducting gap.

The similar scaling number in these two materials supports that the tunnelling spectrums on the ordered surfaces reflect the intrinsic electron pairing within the Fe-As layer. Since the electron pairing is mainly associated with Fe t_{2g} orbitals[1-3] and the pairing strengths may have an orbital dependence, we analysis the tunnelling paths to these orbitals for each surface. Based on the symmetry group of the single Fe-As trilayer[19] as $Z_2 \otimes D_{2d}$, Fe $d_{xz/yz}$ mainly hybridizes with As $p_{x/y}$ orbital while Fe d_{xy} with As p_z orbital[19,20]. Accordingly, for the Ba(K) surface, which is above the As plane, the tunnelling state mainly come from the Ba(K) s orbital overlapping with the As p_z orbital, thus the tunnelling electrons are mostly from d_{xy} orbital. For the As surface, we find that the surface As p_z orbital hybridizes weakly with d_{xy} orbital but strongly with $d_{xz/yz}$ orbital from the calculations, which may be related with two p_z orbitals forming the π^* antibonding state near the Fermi level after the As dimerization (see supplementary), so the tunnelling electrons are mainly from $d_{xz/yz}$ orbital. For the Li surface, the Li-As states

are heavily mixed due to their much smaller distance, thus the Li s orbital overlaps well with all As p orbitals[21] and the tunnelling selects both the d_{xy} and $d_{xz/yz}$ orbitals.

Based on the above orbital hybridization analysis, the phenomenon of surface-dependent gap structures actually demonstrates the orbital feature of the electron pairing as marked in Fig. 4a. It is also meaningful to compare our 'orbital-resolved' gap structures at real space with the study in momentum space. Considering that c-axis tunnelling states mainly carries a small in-plane momentum, we focus on the α and β bands (the inner and outer hole pockets, respectively) for the comparison. Figure. 4b shows the symmetrized spectral intensity of these two bands[4,5] measured by angle resolved photoemission spectroscopy (ARPES), together marked with their dominate d orbital characters[22-24]. It is remarkable that our STS study and the ARPES data have the same results on both the gap magnitudes and their respective orbital characters.

Finally, our real-space characterization on these electronic properties of the stoichiometric Fe-As layer also offers an indispensable reference to understand the impurity effect when adding dopants in this critical layer. For instance, previously we have reported a much shallow and incoherent superconducting gap structure on Ba surface compared with that on As surface for Co-doped Ba122 system[6]. Based on current knowledge, we can infer from these data that the Co dopant mainly cause impurity scattering in the d_{xy} orbital channel in the superconducting state. Such interpretation resonates with the APRES study in the normal state that Co dopants

significantly broaden the width of the band with d_{xy} orbital[24]. Eventually, we believe combining the orbital related information in the space and momentum will provide us a comprehensive understanding on the orbital nature of the iron based superconductivity.
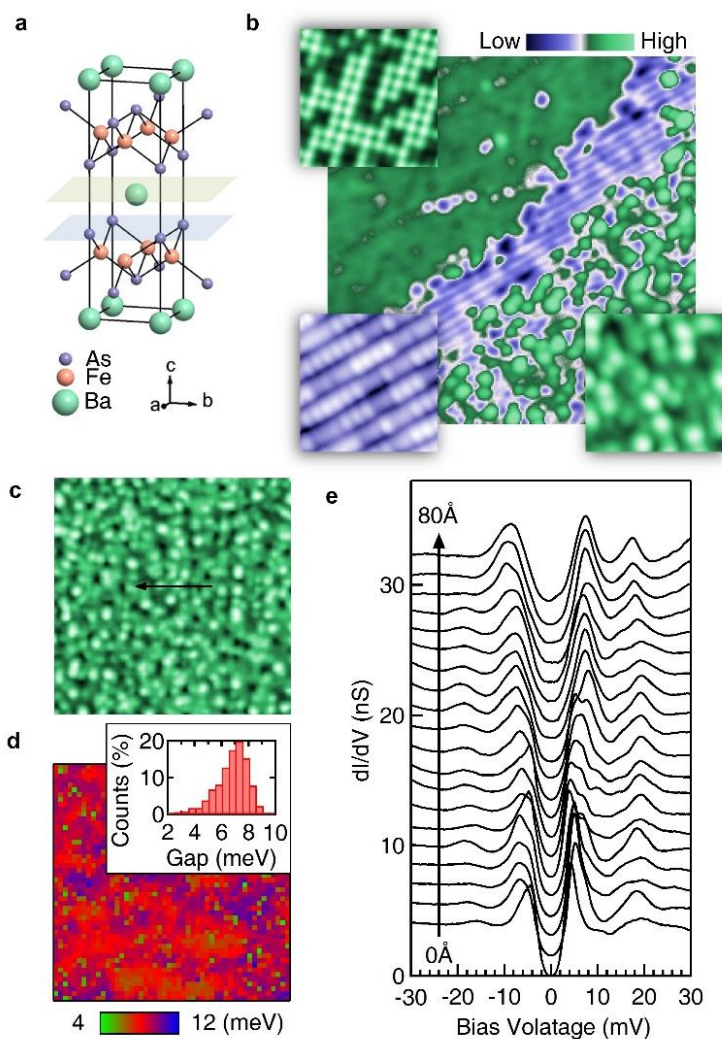

Figure 1 | Cleaving surfaces of $Ba_{0.6}K_{0.4}Fe_2As_2$ and STS on the disordered surface. a, Crystal structure of $BaFe_2As_2$. **b,** A topographic image shows three kinds of surfaces (V = -100 mV, I = 0.3 nA, 300 ×300 Å). A zoom-in image at the left upper corner shows the Ba(K) rt2 surface (V = -50 mV, I = 0.3 nA, 50×50 Å). A zoom-in image at the left lower corner shows the As dimmer row surface (V = -30 mV, I = 0.3 nA, 50 ×50 Å). A

zoom-in image at the right lower corner shows the disordered surface (V = -50 mV, I = 0.3 nA, 50 × 50 Å). **c, d**, Topographic image of a disordered surface (V = -100 mV, I = 0.03 nA, 300 × 300 Å) and its gap-map (V = -20 mV, I = 1nA). **e**, Line-cut spectra along the arrow-line in **c**. Spectra are offset for clarity. All the data are acquired at 4.2 K.
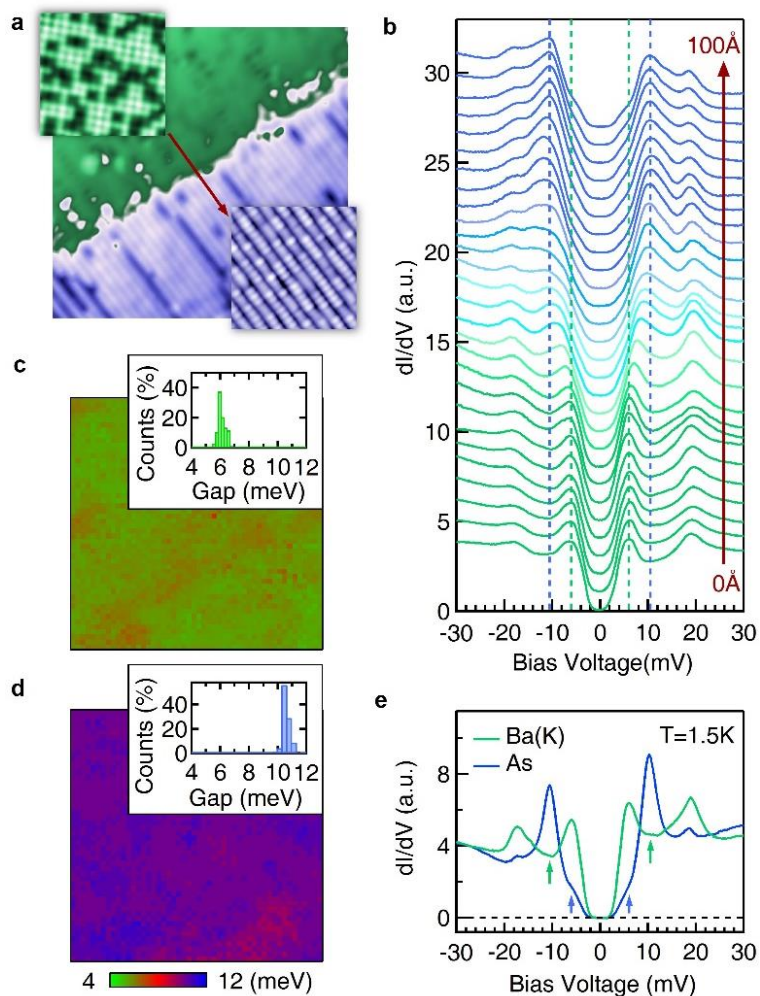

Figure 2 | STS on ordered Ba(K) and As surfaces. a, Topographic image near the boundary between the ordered Ba(K) surface (left upper area) and As surface (right lower area) (V = -100 mV, I = 0.03 nA, 300 × 300 Å, T = 4.2K). A zoom-in image at the left upper corner shows the Ba(K) rt2 surface (V = -50 mV, I = 0.3 nA, 80 × 80 Å). A zoom-in image at the right lower corner shows the As dimmer row surface (V = -30 mV, I = 0.3 nA, 80 × 80 Å). **b**, Line-cut spectra through the surface boundary as marked in

a. Spectra are offset for clarity. **c**, **d**, Gap-map for the ordered Ba(K) and As surface (V = -30 mV, I = 1 nA, 100 × 100 Å, T = 4.2K), respectively. **e,** Spectrums taken on the Ba(K) and As surfaces (V = -30 mV, I = 1 nA, T = 1.5 K).
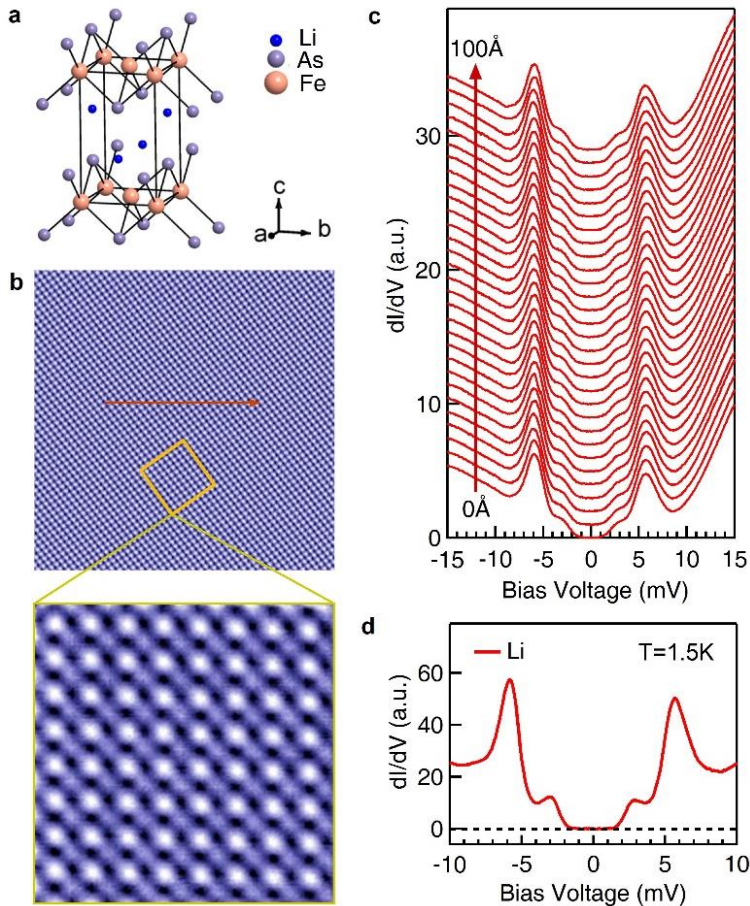

Figure 3 | STS on surface of LiFeAs. **a**, Crystal structure for LiFeAs. **b**, Topographic image of the Li surface (V = -100 mV, I = 1 nA, 200 × 200 Å, T = 4.2 K). High resolution zoom-in image showing both the Li and As atoms (V = -10 mV, I = 0.5 nA, 40 × 40 Å, T = 4.2 K). **c**, Line-cut spectra taken on the Li surface in **b** (V = -15 mV, I = 0.5 nA, T = 4.2 K). Spectra are offset for clarity. **d**, Spectrum taken on the Li surface (V = -15 mV, I = 0.5 nA, T = 1.5 K).
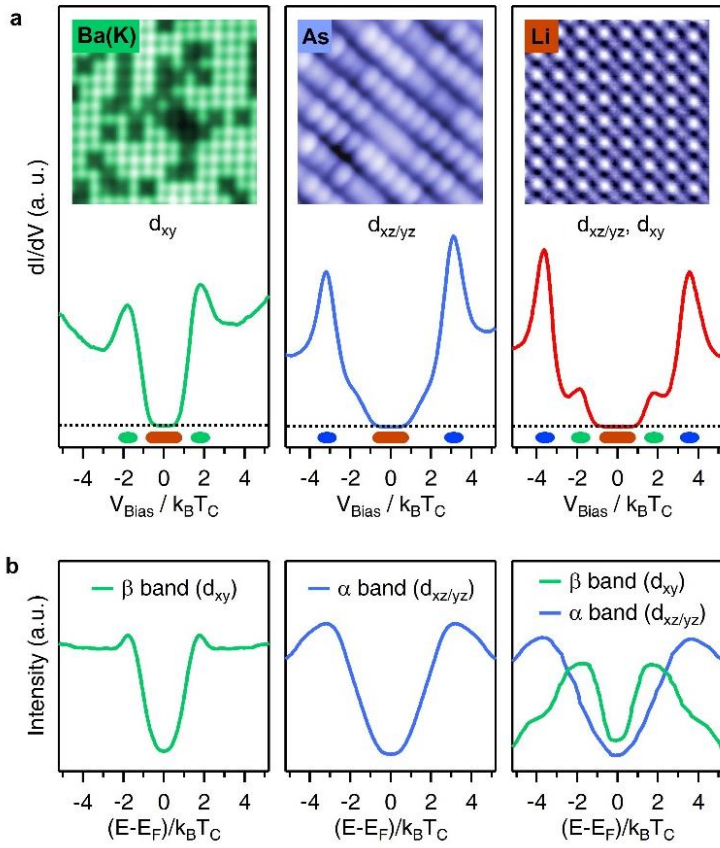
Figure 4 │ Orbital-dependence of superconducting gap structure in space and momentum. a, STS spectra in the energy unit of $k_B T_C$ on three different kind of surfaces taken at 1.5 K. The red bars mark the flat bottom range, the green/blue bars estimate the anisotropy range of the small/large gap. The inset images show the corresponding surfaces, respectively. **b,** Symmetrized ARPES spectra in the energy unit of $k_B T_C$ for β band in $Ba_{0.6}K_{0.4}Fe_2As_2$ (T = 10 K, ref. 4), α band in $Ba_{0.6}K_{0.4}Fe_2As_2$ (k_Z averaged, T = 10 K, ref. 4), and both bands in LiFeAs (T = 8 K, ref. 5), respectively.

References:

1. Singh, D. J. & Du, M. H. Density Functional Study of LaFeAsO$_{1-x}$F$_x$: A Low Carrier Density Superconductor Near Itinerant Magnetism. *Phys. Rev. Lett.* **100**, 237003 (2008).

2. Kuroki, K. *et al.* Unconventional Pairing Originating from the Disconnected Fermi Surfaces of Superconducting LaFeAsO$_{1-x}$F$_x$. *Phys Rev Lett.* **101**, 087004 (2008).

3. Graser, S., Maier, T. A., Hirschfeld, P. J. & Scalapino, D. J. Near-degeneracy of several pairing channels in multiorbital models for the Fe pnictides. *New J. Phys.* **11**, 025016 (2009).

4. Xu, Y. -M. *et al.* Observation of a ubiquitous three-dimensional superconducting gap function in optimally doped Ba$_{0.6}$K$_{0.4}$Fe$_2$As$_2$. *Nat. Phys.* **7**, 198 (2011).

5. Umezawa, K. *et al.* Unconventional Anisotropic s-Wave Superconducting Gaps of the LiFeAs Iron-Pnictide Superconductor. *Phys. Rev. Lett.* **108**, 037002 (2012).

6. Li, Ang *et al.* Surface terminations and layer-resolved spectroscopy in 122 iron pnictide superconductors. Arxiv: XXX.

7. Pickett, W. E. Electronic structure of the high-temperature oxide superconductors. *Rev. Mod. Phys.* **61**, 433 (1989).

8. Shan, Lei *et al.* Evidence of multiple nodeless energy gaps in superconducting Ba$_{0.6}$K$_{0.4}$Fe$_2$As$_2$ single crystals from scanning tunneling spectroscopy. *Phys. Rev. B* **83**, 060510(R) (2011).

9. Shan, Lei *et al.* Observation of ordered vortices with Andreev bound states in Ba$_{0.6}$K$_{0.4}$Fe$_2$As$_2$. *Nat. Phys.* **7**, 325 (2011).

10. Shan, Lei *et al.* Evidence of a Spin Resonance Mode in the Iron-Based Superconductor $Ba_{0.6}K_{0.4}Fe_2As_2$ from Scanning Tunneling Spectroscopy. *Phys. Rev. Lett.* **108**, 227002 (2012).

11. Shun, C. S. *et al.* Scanning Tunneling Spectroscopy of Superconducting LiFeAs Single Crystals: Evidence for Two Nodeless Energy Gaps and Coupling to a Bosonic Mode. *Phys. Rev. Lett.* **109**, 087002 (2012).

12. Allan, M. P. *et al.* Anisotropic Energy Gaps of Iron-Based Superconductivity from Intraband Quasiparticle Interference in LiFeAs. *Science* **336**, 563 (2012).

13. Grothe, S. et al. Bound states of defects in superconducting LiFeAs studied by scanning tunneling spectroscopy. *Phys. Rev. B* **86**, 174503 (2012).

14. Hoffman, J. E. Spectroscopic scanning tunneling microscopy insights into Fe-based superconductors. *Rep. Prog. Phys.* **74**, 124513 (2011).

15. Ding, H. *et al.* Observation of Fermi-surface-dependent nodeless superconducting gaps in $Ba_{0.6}K_{0.4}Fe_2As_2$. *Europhys. Lett.* **83**, 47001 (2008).

16. Lee, Jinho *et al.* Interplay of electron–lattice interactions and superconductivity in $Bi_2Sr_2CaCu_2O_{8+\delta}$. *Nature* **442**, 546-550 (2006).

17. Wang, Zhenyu *et al.* Close relationship between superconductivity and the bosonic mode in $Ba_{0.6}K_{0.4}Fe_2As_2$ and $Na(Fe_{0.975}Co_{0.025})As$. *Nat. Phys.* **9**, 42–48 (2013).

18. Johnston, D. *et al.* The Puzzle of High Temperature Superconductivity in Layered Iron Pnictides and Chalcogenides. *Advances in Physics* **59**, 803 (2010).

19. Hu, J.-P. Iron-Based Superconductors as Odd-Parity Superconductors. *Phys. Rev. X* **3**, 031004 (2013).

20. Zhou, S., Kotliar, G. & Wang, Z. Extended Hubbard model of superconductivity driven by charge fluctuations in iron pnictides. *Phys. Rev. B* **84**, 140505(R) (2011).

21. Lankau, Alexander *et al.* Absence of surface states for LiFeAs investigated using density functional calculations. *Phys. Rev. B* **82**, 184518 (2010).

22. Wang, X. -P. Orbital characters determined from Fermi surface intensity patterns using angle-resolved photoemission spectroscopy. *Phys. Rev. B* **85**, 214518 (2012).

23. Evtushinsky, D. V. *et al.* Strong pairing at iron $3d_{xz,yz}$ orbitals in hole-doped $BaFe_2As_2$. *Phys. Rev. B* **89**, 064514 (2014).

24. Ye, Z. R. *et al.* Extraordinary quasiparticle scattering and bandwidth-control by dopants in iron-based superconductors. *Phys. Rev. X* **4**, 031041 (2014).

Author contributions:

J.X.Y., Z.W. J.H.W. and A. L. carried out the STM/S experiments with contributions from X.J.L. and P. H. H; X. X. W. preformed the first principle calculations; C.L.Z, P.C.D. and G.F.C. synthesized and characterized the $Ba_{0.6}K_{0.4}Fe_2As_2$ samples; X.C.W. and J.X.Y. synthesized and characterized the LiFeAs samples; J.X.Y., J.L, J.P. Hu, Z.Q.W., S.H.P. and H.D. performed the data analysis, figure development and wrote the paper; S.H.P. supervised the project. All authors have discussed the results and the interpretation.

Supplementary

First principle calculation

Our first principle calculations employ the projector augmented wave method encoded in Vienna ab initio simulation package[25-27], and the generalized-gradient approximation for the exchange correlation function is used[28]. The cutoff energy of 500 eV is taken for expanding the wave functions into plane-wave basis. In the calculation, the Brillouin Zone is sampled in the k space within Monkhorst-Pack scheme[29]. The number of these k points is ($6 \times 11 \times 1$) for the 2×1 As-terminated surface. We modeled a surface using a slab of six FeAs layers and five Ba layers plus a vacuum layer of 20Å with inversion symmetry through the center of the slab. To model the observed 2×1 As-terminated surface in experiment, we move the two neighboring surface As atoms closer by 20% (as estimated from the experiment[14]) along **a** axis.

In $BaFe_2As_2$, the strong coupling between the p_z orbitals of the interlayer As ions makes the band dispersive along **c** axis. The coupling between Ba and As ions is also mainly attributed to As p_z orbitals. Therefore, we expect the cleaving has great effect on p_z orbitals but little effect on p_x and p_y orbitals for As ions on the explosed surface. The projected density of states (DOS) of two surface As ions (AsS1 and AsS2 for top and down As ions of the surface FeAs trilayer respectively) and one bulk As ion (AsB) are shown in Fig. S1. The p states of bulk As are mainly located in the energy region from -5.0 eV to -2.0 eV. The p_x and p_y orbitals are split for the surface As ions, which is due to the C_4 symmetry breaking caused by the As dimerization. Compared with bulk As ions, the p_x and p_y states of surface As ions have little changes but an energy shift. However, the p_z orbitals of the surface AsS1 become much more extended compared

with the bulk As ions. Furthermore, the AsS1 p_z states are strongly enhanced near the Fermi level. On the other hand, the p_z states of the AsS2 resemble the bulk one.

The states of the superconducting gap related Fe orbitals (d_{xz}, d_{yz}, d_{xy}) and As p_z orbitals are shown in Fig. S2 for Fe ions both in the bulk and on the surface (note that we choose the surface Fe ion to be the one just below an As dimmer). Now, we focus on the states near the Fermi level. In the bulk, the peak of As p_z orbitals matches with that of d_{xy} orbitals and avoids that of $d_{xz/yz}$ orbitals near the Fermi level in Fig. S2(a). It indicates that As p_z orbitals couple strongly with Fe d_{xy} as required by symmetry. On the contrary, the peaks of surface As p_z orbitals avoid those of d_{xy} orbitals but match with those of $d_{xz/yz}$ orbitals as marked in the orange shaded area in Fig. S2(b). We conclude that surface p_z orbitals should hybridize weakly with Fe d_{xy} orbitals but could hybridize with $d_{xz/yz}$ orbitals.

Finally, we discuss the possible explanations of the above surface effects. The surface As ions are electron deficient after the cleaving due to the absence of Ba ions. Then the surface As ions tend to bond with the surrounding As ions, forming As dimers. As the electron deficiency happens mainly within the p_z orbitals of surface As, the bonding should mainly involve the p_z orbitals, forming a π bonding state and a π* antibonding state as shown in Fig. S3(a). Fig. S3(b)-(e) show the projection of $d_{xz/yz}$, d_{xy}, π and π* orbitals in the **a-c** plane. As can be seen, the π state could couple with d_{xy} but not $d_{xz/yz}$ while the π* state could couple with $d_{xz/yz}$ but not d_{xy}. In Fig. S2(b), based on the position

of their maximum DOS peaks, we find that the surface As p_z orbitals couple with d_{xy} orbitals but weakly with $d_{xz/yz}$ below -1.5 eV, while the surface As p_z orbitals couple weakly with d_{xy} orbitals but could couple with $d_{xz/yz}$ orbitals near the Fermi level. This surface effect is in sharp contrast with the coupling between Fe and As in the bulk, but is consistent with our analysis in Fig. S3. Hence, the corresponding π bonding state is located below -1.5 eV and the π^* antibonding state is near the Fermi level for the plotted surface p_z orbital in Fig. S2(b).
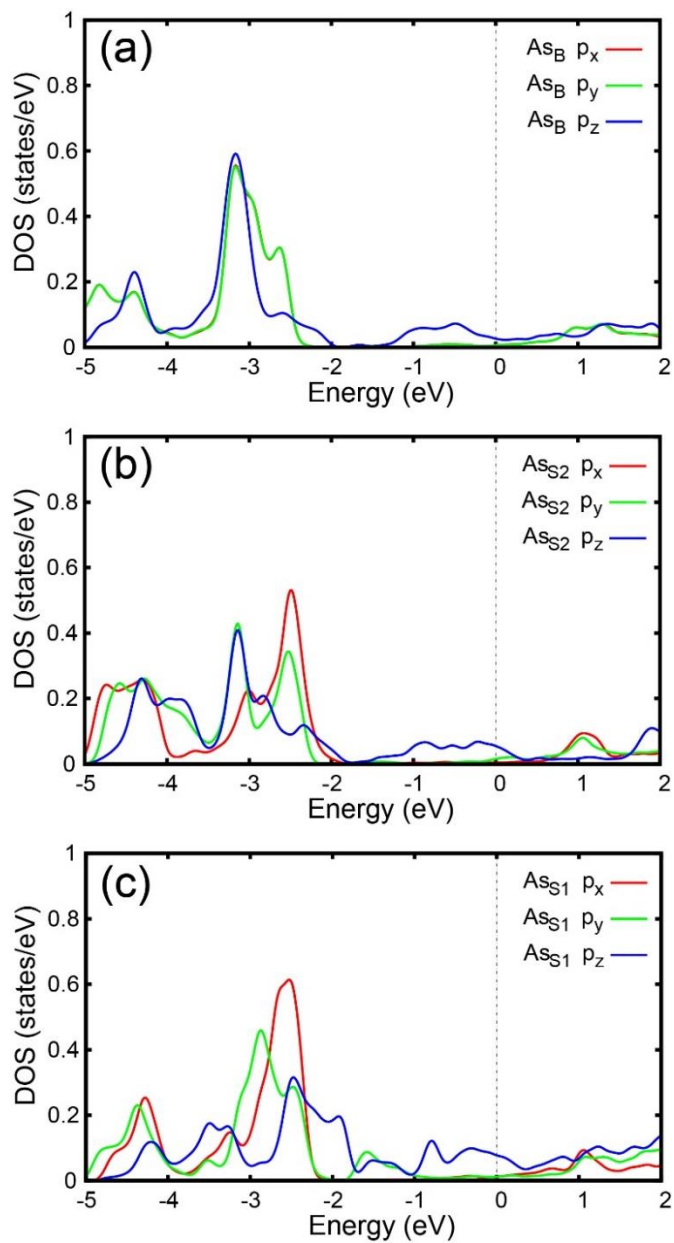
Figure. S1: Projected DOS of bulk As and surface As ions. (a) bulk As (b) the bottom As ions of the surface FeAs trilayer (c) the top As ions of the surface FeAs trilayer.
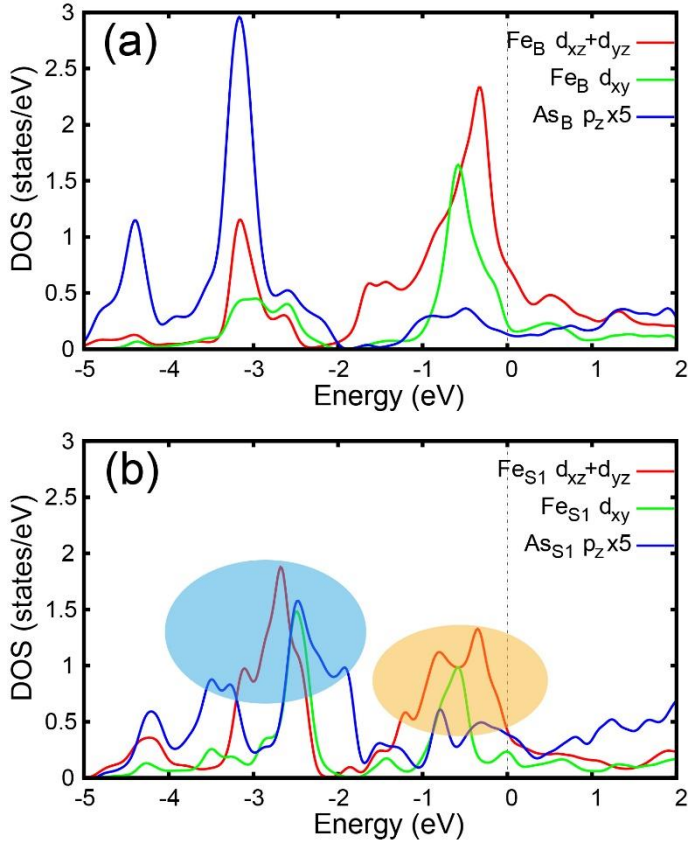
Figure. S2: The project DOS of bulk and surface Fe and As ions. (a) the bulk Fe and As (b) the surface Fe and As. Only the superconducting gap related Fe orbitals are shown. The orange and blue shaded stand for the π^* antibonding and π bonding state region, respectively. The DOS of p_z orbitals is scaled by a factor of 5.0.
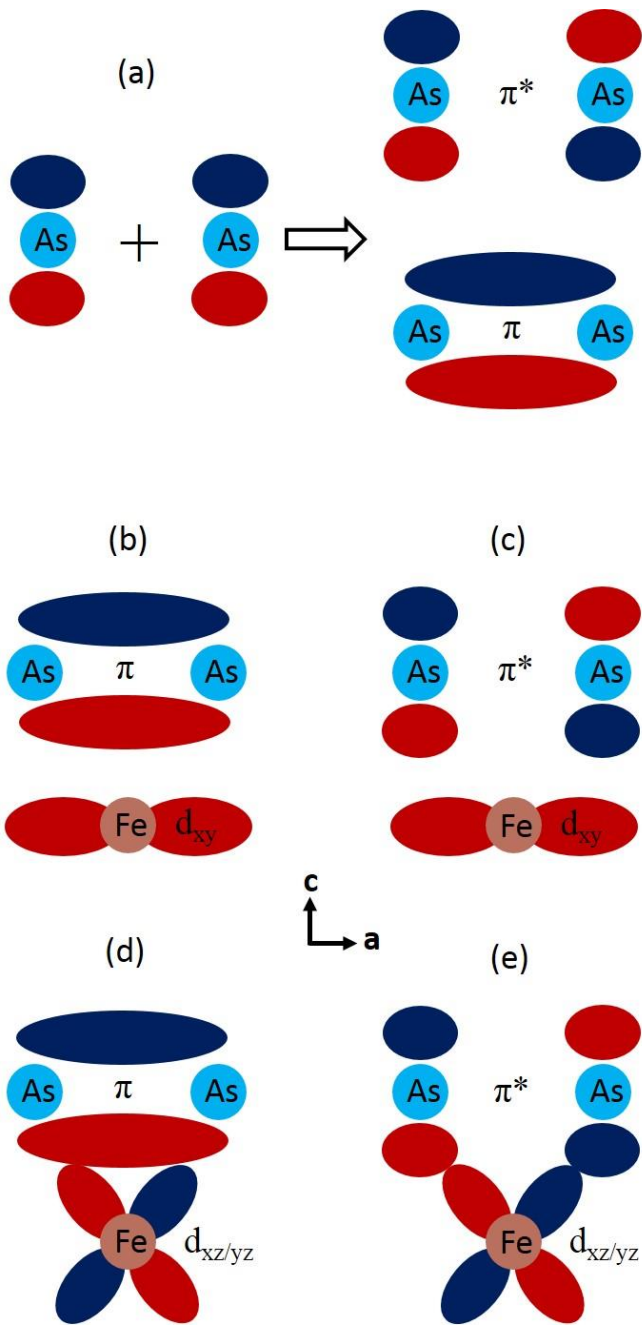
Figure. S3: Cartoon of the coupling between d_{xy}, $d_{xz/yz}$ orbitals and π, π^* orbitals projected in the **a-c** plane. (a) Illustration of π bonding and π^* antibonding orbitals formation when two p_z orbitals hybridize. (b)-(e) Coupling between d_{xy} and π orbitals, d_{xy} and π^* orbitals, $d_{xz/yz}$ and π orbitals, $d_{xz/yz}$ and π^* orbitals, respectively. The light blue circles and light red circles represent As and Fe ions respectively. The dark blue and dark red color illustrate the opposite phases of the orbital function.

1. Kresse, G. & Hafner, J. Ab *initio* molecular dynamics for liquid metals. *Phys. Rev. B* **47**, 558 (1993).

2. Kresse, G. & Furthmuller, J. Comput. Efficiency of ab-initio total energy calculations for metals and semiconductors using a plane-wave basis set. *Mater. Sci.* **6**, 15 (1996).

3. Kresse, G. & Furthmuller, J. Efficient iterative schemes for *ab initio* total-energy calculations using a plane-wave basis set. *Phys. Rev. B* **54**, 11169 (1996).

4. Perdew, J. P., Burke, K. & Ernzerhof, M. Generalized Gradient Approximation Made Simple. *Phys. Rev. Lett.* **77**, 3865 (1996).

5. Monkhorst, H. J. & Pack, J. Special points for Brillouin-zone integrations. *Phys. Rev. B* **13**, 5188 (1976).